Int. J. Simul. Multidisci. Des. Optim. **14**, 19 (2023)
© K. Muniyappan and L. Nagarajan, Published by EDP Sciences, 2023
https://doi.org/10.1051/smdo/2023021

IJSMDO
Available online at:
https://www.ijsmdo.org

RESEARCH ARTICLE OPEN ACCESS

Parameter optimization of titanium-coated stainless steel inserts for turning operation

Karthick Muniyappan* and Lenin Nagarajan

Department of Mechanical Engineering, Vel Tech Rangarajan Dr. Sagunthala R&D Institute of Science and Technology, Avadi, Chennai − 600062, Tamil Nadu, India

Received: 10 April 2023 / Accepted: 12 November 2023

Abstract. This study discusses the three essential process parameters cutting speed, feed and depth of cut on the quality of the tool during turning operation. A high-strength stainless steel tool coated with tungsten carbide is used. The tool is further strengthened using cryogenic treatment by immersing it in liquid nitrogen for 24 h and 36 h respectively. The surface roughness of the simple coated tool and the processed tool is compared using optimization techniques like the Taguchi technique and ANOVA. The analysis revealed that the surface roughness of the simple coated tool insert was 0.5 μm, whereas the surface roughness of the tool inserts immersed in liquid nitrogen for 36 h was 12.5 μm. The processed tool insert became brittle which lead to an increase in surface roughness after the turning operation. Three different algorithms like Grass Hopper Optimization, Moth Flame Optimization, and Salp Swarm Optimization were used to observe the feasibility of the optimization techniques. The Moth Flame Optimization algorithm had good convergence and also delivered results that were correlating with the ANOVA. It is concluded that while keeping a high tool rotation speed of 984.46 rpm, a low feed of 91.4 mm/min and a depth of cut of 0.25 mm resulted in a low surface roughness of simple coated tool insert was 0.59 μm.

Keywords: Coated tool insert / turning / optimization techniques / surface roughness

1 Introduction

The turning operation is a metal-cutting process that is used to remove excess materials and also produces desired shapes in a given part. The turning operations can be semiautomatic as in the case of lathe machines or can be fully automated with the help of computerized turning machines. A single-point cutting tool is used to carry out the turning operation. Typically, the cutting tool is held stationary in a vice or tool holder while the material is made to rotate along a fixed axis. The pointed tool removes a small layer of the rotating material while performing the turning operation. The quality of the turning operation and smoothness of the finished workpiece depends on factors like rotation, depth of cut, and cutting force. The turning operation is a traditional metal cutting operation that has been performed ever since the industrial revolution and the invention of the lathe. According to Yadav et al. [1], machining parameters like spindle speed, feed, and depth of cut influence the change in hardness caused on the material surface due to turning operations. In the experiments, EN 8 metal was used as the workpiece, and coated carbide tools were used as the tools. The hardness after turning was measured on the Rockwell scale. Several turning parameters were optimized by Shivade et al. [2] for turning on EN8 steel using a single response optimization method. Taguchi's L9 Orthogonal array design is used in experiments. In this paper, an investigation into the use of the Taguchi parameter is discussed. In their work [2], they optimized Surface Roughness and Tool tip temperature in turning operations using single-point carbide cutting tools.

During turning operations on various steel grades, Deshpande et al. [3] reviewed various parameters like surface roughness, MRR, and tool wear. Cutting speed, feed rate, depth of cut, and tool wear were some of the turning input parameters in various papers, while surface roughness, cutting forces, tool wear and MRR were some of the output parameters. The Taguchi and RSM approaches have been used in several research studies to design and optimize parameters. Using tungsten-coated carbide tools to turn Aluminum Alloy 7075, Alagarsamy et al. [4] describe Taguchi design of experiments methodology. A standard orthogonal array design based on L27 provides three process parameters for material removal rate and machining time, which are cutting speed, feed, and depth of

* e-mail: karthick@veltech.edu.in

This is an Open Access article distributed under the terms of the Creative Commons Attribution License (https://creativecommons.org/licenses/by/4.0), which permits unrestricted use, distribution, and reproduction in any medium, provided the original work is properly cited.

cut. Using the physical vapour deposition technique, Lakshmanan et al. [5] fabricated WC inserts with a single-layered AlCrN-based coating. A carbide insert was examined for micro-hardness, coating thickness, surface morphology, and elemental composition. Using conventional and cryogenic coolants (LN2), turning operations were performed on Ti-6Al-4V alloys with coated carbide (AlCrN-cc) and without coated carbide inserts. In an experiment, we measured the roughness value and turning forces for different feeds, depths of cuts, and cutting speeds.

According to Ezugwu et al. [6], titanium machining has many problems such as tool wear and failure mechanisms. Straight tungsten carbide (WC/Co) cutting tools continue to remain superior in nearly all titanium alloy machining processes, even though Chemical Vapour Deposition (CVD) coated carbides and ceramics haven't been able to replace cemented carbides as they react with titanium and were relatively low in fracture toughness and thermal conductivity. Xiaoping et al. [7] discuss potential research issues regarding machining titanium and its alloys. Because of their exceptional corrosion resistance and high strength-to-weight ratio, titanium and its alloys are highly attractive materials. Aerospace has been titanium's major application. Researchers Kainz et al. [8] have developed a multi-layered coating architecture that consists of two alternating hard materials that enhance the mechanical properties of hard coatings in the metal cutting industry. CVD TiN/TiBN multilayer coatings were correlated with their microstructures in this work, and they were compared to their single-layer counterparts. A thermal CVD plant prepared multilayers with different bilayer periods (1400, 800, 300, and 200 nm) by varying the composition of the feed gas alternately.

According to Alborz et al. [9], cryogenic milling has been the focus of their research. End milling Ti–6Al–4V titanium alloy with cryogenic cooling and conventional dry and flood cooling is compared. Various combinations of cutting parameters were tested in machining experiments. Micro-hardness was measured for each sample under subsurface conditions and surface roughness was examined. In a milling experiment with various nose radiuses, Emel [10] found that adhesion, abrasion, chipping, and fracture are the main mechanisms and modes of tool failure. Regardless of cutting speed and milling direction, cutting forces decreased with an increase in nose radius, excluding up-milling at cutting speed over 90 m/min. It was observed that roughness decreased with increasing nose radius and speed in the experiments. Up milling resulted in lower surface roughness and forces than down milling. The study revealed that the increase in nose radius caused an increase in edge serration in chip morphology.

Fernandez-Valdivielso et al. [11] proposed a new testing method to detect the important dimensional parameters and grades of carbide inserts for turning of nickel alloys regarding surface reliability. Gandarias et al. [12] discussed the controversy surrounding the cryogenic treatment of steels. Though cryogenic treatment is effective in some cases, such as in HSS steels, its effectiveness in carbide inserts is still debated. Pereira et al [13] discussed the cryogenic treatment of AP23 steel using carbon dioxide. They inferred that the tool life increased by 12% and the surface roughness decreased after subjecting the tool to cryogenic treatment. Polvorosa et al. [14] in their study presented, the results recorded during turning operations to find flank and notch wear were summarized, using cooling at above 5 bars. They inferred that large-grain alloy indicates high-notch wear. However, smaller grain size results in high flank wear. Amigo et al. [15] predicted the cutting force and tool wear during high-speed turning of Nimonic superalloy. With cutting speeds lower than 100 m/min, the wear prediction model produced relative errors of less than 5%, and with speeds higher than 100 m/min, it produced errors of less than 14%. By increasing tool life x3 (from 8 to 24 min), reducing the side cutting edge angle also contributed to the improvement in tool life. A study conducted by Zhang et al. [16] discussed the use of in-process stochastic tool wear identification as a method for improving micro milling force modelling. To predict stochastic tool wear values, they proposed improving the integrated estimation technique based on the long short-term memory (LSTM) network and particle filter algorithm. By considering the influence of tool wear, they found that micro-cutting tool availability and sustainability have improved, and prediction accuracy has increased by 3.4% as well.

Sivalingam et al. [17] carried out the optimization of process parameters for various machining environments using an evolutionary algorithm. Three different case studies were considered during their study. A comparison was made between the MFO algorithm and genetic algorithms, grasshopper algorithms, grey wolves, and particle swarm optimization algorithms in order to evaluate the effectiveness of the MFO algorithm. The results showed that the MFO algorithm outperformed the other algorithms in terms of performance.

Dhilip et al. [18] discussed on turning of hardened non-shrinking die steel having Rockwell hardness of 45 to 70. They attempted to maximize the material removal rate with minimal machining time and surface roughness. Optimization was carried out using the L9 algorithm. Grey relational analysis was used for optimizing the output characteristics.

Rana [19] optimized the machining performance of CNC tool inserts coated with tungsten carbide coating under dry cutting. The coating was carried out using the CVD method. The average evaluated Vickers Hardness was found to be 1455HV and 951HV for both coated as well as uncoated samples respectively. This shows a 53% rise in the hardness of the uncoated tungsten carbide inserts.

Das et al. [20] used machine learning to optimize the turning capability of AISI D6 steel. There are various ML approaches that can be used to model different response variables, including polynomial regression, random forest regression, gradient boosted trees, and adaptive boosting regression based on adaptive boosting. The complexity of the models was suited to optimize the turning characteristics with high accuracy. However, the calculations demanded high-end computing systems to finish the calculation within a reasonable time.

Sobh et al. [21] used the Taguchi technique to optimize the turning parameters of the titanium alloy tool insert. Three levels of cutting parameters were used in the

experiment, each with three different levels, so that three different cutting parameters could be varied. A variety of cutting speeds were experimented with, such as 80, 100, and 120 m/min, variable feed rates were used, such as 0.05, 0.1, and 0.15 mm/rev, and variable cutting depths were varied as 0.2, 0.4, and 0.6 mm, respectively. There were two significant parameters that appear to be important in determining the level of surface roughness and wear of the tool inserts: the cutting speed and the cutting depth.

The surface roughness of AISI steel inserts coated with CVD coatings was optimized based on the turn parameters and the insert geometry of Vukelic et al. [22]. In order to achieve the best results, the machined parts were machined at various speeds, feed rates, depths of cut, corner radiuses, rakes, as well as angles of approach and inclination. In order to derive an empirical, regression model for arithmetical mean surface roughness, the roughness of the surface was measured after each experiment, and statistical analysis was used to generate the model. The results of the study demonstrate that the developed model can be applied in a practical manner.

In a review of tool life optimization and their effectiveness on tool inserts, Kamble et al. [23] presented a review of tool life optimization. For the purpose of predicting the life of tools, a variety of methods and approaches have been considered here, such as Taguchi methods and regression analyses. They concluded that the Taguchi technique using the observations in regression analysis can effectively calculate the feed rate and depth of cut constants and also the tool life.

Using cryogenically treated tools in hardened hot work tool steel turning, Nas and Zbek [24] conducted an investigation into optimizing the machining parameters through the use of cryogenically treated tool materials. They optimized their performance using Taguchi L18, a method that was developed based on gray relational analysis with Taguchi L18. Dry turning tests were performed using carbide cutting tools that had been cryogenically treated as well as those that had not been treated. According to the results of the analysis, the feed rate (72.84%) was identified as the dominant factor that affected surface roughness and the cutting speed (93.93%) was identified as the dominant factor that affected flank wear.

During the side milling of DAC 55 steel, Tomadi et al. [25] performed an optimization analysis on the size of the cut and the radius of the cutting edge during the side milling process. During the machining operation, they aimed to optimize both the radius of the cutting edge of the tools as well as the width of the cut when the tools were used. The width of the cut appears to have the greatest influence on the quality of the surface roughness when compared to the radius of the cutting edge when it comes to improving the quality of the surface roughness.

Akgun and Kara [26] through optimization techniques analysed the cutting tool coating effect on surface roughness and cutting force during the turning of AA6061. TiB_2 was coated on the tool insert using PVD technique. The mathematical models for the cutting force and surface roughness were developed through linear and quadratic regression models. The results indicated that the best performance in terms of Fc and Ra was obtained at an uncoated insert, cutting speed of 350 m/min, feed rate of 0.1 mm/rev, and depth of cut of 1mm. Moreover, the feed rate is the most influential parameter on Ra and Fc, with 64.28% and 54.9%, respectively.

Arunkarthikeyan and Balamurugan [27] used multi objective optimization technique to find the performance improvement of cryo treated inserts on turning of AISI 1018 steel. Dry turning operation was conducted according using Taguchi's L9 orthogonal array using 3 factors and 3 levels to find the tool wear rate and surface roughness. They suggested that MRGRA gives better results on cryo treated WC-Co inserts when machining of AISI 1018 steel.

Several pieces of literature pointed out the influence of the turning tool parameters on the finishing quality of the turned workpieces. Studies made on tool inserts revealed that operating parameters like tool geometry, material being machined, and effectiveness of coolant determine the operating life of the tool. Optimization techniques were carried out to improve the machining capability of the tool inserts without sacrificing their service life. However, there are other qualities like the strength of the tool, its tribological property and corrosion that also influences the quality of the turning operation. In this paper multi-criteria decision-making approach is adopted to optimize the parameters that deliver a good finish turning on the workpiece. The experiment is carried out using a tungsten carbide-coated stainless-steel tool insert. The coated insert is subjected to hardening under cryogenic temperature. The surface roughness of the tool insert after the turning operation is optimized. A reliable optimization technique is selected and optimized parameters are determined through this study.

2 Materials and methods

2.1 Experimental setup

For the experiment, a custom-450 grade stainless steel of diameter 89 mm and length 510 mm is used. The tool insert is coated with tungsten carbide (WC). The coating is carried out through the electroplating method till the 650 nm layer of the tungsten carbide was deposited over the stainless steel. The coating is strengthened with the help of cryogenic treatment. For this, the coated tool insert was dipped in liquid nitrogen. Three different approaches were used in this experiment. At first, the electro-coated tool insert without any post-treatment is considered. Secondly, the coated tool insert is subjected to cryogenic treatment by dipping the insert in liquid nitrogen for 12 h. Finally, the coated tool insert is subjected to cryogenic treatment by dipping the insert in liquid nitrogen for 36 h. The tool inserts thus produced and subjected to cryogenic treatment are used to carry out turning operations on mild steel workpieces. After that, the surface roughness of the tool insert is determined. The surface roughness of the coated tool inserts (Ra), 12 h cryogenically treated insert (Rq), and 36 h cryogenically treated insert (Rz) are found using optimization techniques.

Table 1. L27 array and values of the turning parameters.

N	F	D	Ra	Rq	Rz
850	60	0.25	0.749	0.817	3.576
850	60	0.5	0.986	1.159	5.362
850	60	0.75	1.136	1.595	7.524
850	120	0.25	1.140	1.262	5.168
850	120	0.5	1.481	1.379	5.711
850	120	0.75	1.316	1.573	6.225
850	180	0.25	2.464	2.937	11.678
850	180	0.5	2.498	2.983	11.857
850	180	0.75	2.974	3.148	12.742
950	60	0.25	0.594	0.731	2.539
950	60	0.5	0.883	1.143	5.294
950	60	0.75	1.006	1.456	8.022
950	120	0.25	0.895	1.070	4.403
950	120	0.5	1.004	1.213	5.102
950	120	0.75	1.228	1.528	4.291
950	180	0.25	1.894	2.336	9.273
950	180	0.5	1.988	2.456	9.798
950	180	0.75	2.368	2.870	12.409
1050	60	0.25	0.500	0.624	3.105
1050	60	0.5	0.867	1.190	5.825
1050	60	0.75	1.322	1.677	9.119
1050	120	0.25	0.821	0.961	3.786
1050	120	0.5	1.298	1.429	5.058
1050	120	0.75	0.915	1.479	4.376
1050	180	0.25	1.892	2.219	8.444
1050	180	0.5	2.101	2.477	9.666
1050	180	0.75	2.145	2.273	9.349

2.2 Optimization using Taguchi technique

Optimization is conducted using Taguchi's L27 orthogonal array technique. In the L27 array, thirteen columns are used to tabulate the experimental parameters and their correlation. For the three-factor three-level experiment set, the total number of experiments that should be carried out is 27. These experimental combinations were carried out for all three sets of inserts. In this study, three different control factors with three different levels. The turning operation was carried out on a centre lathe with variable speed and feed drive with a tool dynamometer setup as a force measurement device. For each experiment, a fresh cutting edge is used. Each machining operation is carried out for 1 min of duration. For each experiment, the feed force (Fx), thrust force (Fy), and cutting force (Fz) are tabulated by means of a piezoelectric tool post dynamometer. The surface roughness value for each machined surface is found precisely using a probe-type surface roughness tester. The control factors were cutting speed (N), feed (F) and Depth of cut (D). Table 1 shows the values assigned to the three different parameters. The cutting speed is varied from 850 pm to 1050 rpm. The feed is varied from 60 mm/min to 180 mm/min. The depth of cut is varied from 0.25 mm to 0.75 mm. The surface roughness is measured in μm.

2.3 Optimization using ANOVA technique

The surface roughness of the coated tool inserts (Ra), 12h cryogenically treated insert (Rq), and 36h cryogenically treated insert (Rz) is determined using the ANOVA technique. Equation (1) shows the regression equation used for Ra. Table 2 shows that the linear approach is used during ANOVA. It is observed that the p-Value for the model was less than 0.05. This reveals that the ANOVA model is statistically significant and is taken into consideration for the study. Table 3 shows the coefficients obtained during the analysis of Ra. From Table 4 it is found that the model has around 95% fit.

$$\begin{aligned} \mathrm{Ra} &= 17.38 - 0.0295\mathrm{N} + 0.00351\mathrm{F} + 1.48\mathrm{D} \\ &+0.000016\mathrm{N} * \mathrm{N} + 0.000126\mathrm{F} * \mathrm{F} - 0.76\mathrm{D} * \mathrm{D} \\ &-0.000022\mathrm{N} * \mathrm{F} + 0.00032\mathrm{N} * \mathrm{D} - 0.00214\mathrm{F} * \mathrm{D} \end{aligned} \quad (1)$$

Table 2. Analysis of Variance for Ra.

Source	DF	Adj SS	Adj MS	*F*-Value	*P*-Value
Model	9	11.1397	1.23775	50.86	0.000
Linear	3	9.5051	3.16835	130.18	0.000
N	1	0.4619	0.46194	18.98	0.000
F	1	8.3779	8.37787	344.22	0.000
D	1	0.6652	0.66524	27.33	0.000
Square	3	1.4038	0.46793	19.23	0.000
N*N	1	0.1542	0.15420	6.34	0.022
F*F	1	1.2361	1.23611	50.79	0.000
D*D	1	0.0135	0.01348	0.55	0.467
2-Way Interaction	3	0.2309	0.07697	3.16	0.052
N*F	1	0.2178	0.21780	8.95	0.008
N*D	1	0.0008	0.00076	0.03	0.862
F*D	1	0.0123	0.01234	0.51	0.486
Error	17	0.4138	0.02434		
Total	26	11.5535			

Table 3. Coefficients for Ra.

Term	Coef	SE Coef	*v*-Value	*P*-Value	VIF
Constant	14.38	5.85	2.46	0.025	
N	-0.0295	0.0122	-2.43	0.027	1096.00
F	0.00351	0.00846	0.42	0.683	190.37
D	1.48	2.03	0.73	0.475	190.38
N*N	0.000016	0.000006	2.52	0.022	1084.00
F*F	0.000126	0.000018	7.13	0.000	49.00
D*D	-0.76	1.02	-0.74	0.467	49.00
N*F	-0.000022	0.000008	-2.99	0.008	142.37
N*D	0.00032	0.00180	0.18	0.862	142.37
F*D	-0.00214	0.00300	-0.71	0.486	13.00

Table 4. Model Summary for Ra.

S	R-sq	R-sq(adj)	R-sq(pred)
0.156009	96.42%	94.52%	90.30%

Equation (2) shows the regression equation used for Rq. Table 5 shows the F values and P Values measured during ANOVA. It is observed that the *p*-Value for the model was less than 0.05. This reveals that the ANOVA model is statistically significant and is taken into consideration for the study. Table 6 shows the coefficients obtained during the analysis of Rq. From Table 7 it is found that the model has around 97% fit.

$$\begin{aligned} \mathrm{Rq} &= 7.48 - 0.01523\mathrm{N} + 0.00568\mathrm{F} + 1.48\mathrm{D} \\ &+0.000009\mathrm{N} * \mathrm{N} + 0.000159\mathrm{F} * \mathrm{F} - 0.268\mathrm{D} * \mathrm{D} \\ &-0.000028\mathrm{N} * \mathrm{F} + 0.00109\mathrm{N} * \mathrm{D} - 0.00976\mathrm{F} * \mathrm{D} \end{aligned} \quad (2)$$

Equation (3) shows the regression equation used for Rz. Table 8 shows the F values and P Values measured during ANOVA. It is observed that the p-Value for the model was less than 0.05. This reveals that the ANOVA model is statistically significant and is taken into consideration for the study. Table 9 shows the coefficients obtained during the analysis of Rz. From Table 10 it is found that the model has around 90% fit.

$$\begin{aligned} \mathrm{Rz} &= 29.6 - 0.0578\mathrm{N} - 0.0048\mathrm{F} + 8.4\mathrm{D} \\ &+0.000035\mathrm{N} * \mathrm{N} + 0.000885\mathrm{F} * \mathrm{F} - 0.17\mathrm{D} * \mathrm{D} \\ &-0.000145\mathrm{N} * \mathrm{F} + 0.0048\mathrm{N} * \mathrm{D} - 0.0574\mathrm{F} * \mathrm{D} \end{aligned} \quad (3)$$

Three different algorithms are used in this study to arrive at an optimized value of the surface roughness of the tool inserts. The pseudo-code for Grass Hopper Optimization (GHO) algorithm is provided below.

Initialize the swarm Xi (i=1,2,3,....,n)

Initialize C_{max}, C_{min} and ite_{max}

Table 5. Analysis of Variance for Rq.

Source	DF	Adj SS	Adj MS	F-Value	P-Value
Regression	9	14.0051	1.55612	99.86	0.000
N	1	0.0381	0.03809	2.44	0.136
F	1	0.0110	0.01098	0.70	0.413
D	1	0.0122	0.01221	0.78	0.388
N*N	1	0.0461	0.04606	2.96	0.104
F*F	1	1.9657	1.96569	126.15	0.000
D*D	1	0.0017	0.00169	0.11	0.746
N*F	1	0.3396	0.33964	21.80	0.000
N*D	1	0.0089	0.00888	0.57	0.461
F*D	1	0.2572	0.25722	16.51	0.001
Error	17	0.2649	0.01558		
Total	26	14.2700			

Table 6. Coefficients for Rq.

Term	Coef	SE Coef	T-Value	P-Value	VIF
Constant	7.48	4.68	1.60	0.129	
N	-0.01523	0.00974	-1.56	0.136	1096.00
F	0.00568	0.00677	0.84	0.413	190.37
D	1.44	1.62	0.89	0.388	190.38
N*N	0.000009	0.000005	1.72	0.104	1084.00
F*F	0.000159	0.000014	11.23	0.000	49.00
D*D	-0.268	0.815	-0.33	0.746	49.00
N*F	-0.000028	0.000006	-4.67	0.000	142.37
N*D	0.00109	0.00144	0.75	0.461	142.37
F*D	-0.00976	0.00240	-4.06	0.001	13.00

Table 7. Model Summary for Rq.

S	R-sq	R-sq(adj)	R-sq(pred)
0.124830	98.14%	97.16%	94.84%

Calculate the fitness of each agent
T = the best search agent
While ($I < ite_{max}$)
Compute non-dominated solutions
Compute the best solution based on the crowding distance (F_{1j})
Update the achieve size
Update C
For each search agent
Normalize the distance between the grasshoppers
Update the position of current search agent
Bring the current search agent back if it goes outside the boundaries
End for
Update T if there is a better solution
I = I + 1
End While
Print the best solution

The pseudo-code for Moth Flame Optimization (MFO) algorithm is provided below.

Initialize the parameters for Moth-flame
Initialize Moth position Mi randomly
For each *I = 1:n* do
Calculate the fitness function *fi*
End For
While *(iteration ≤ max-iteration)* do
Compute non-dominated solutions
Compute the best solution based on the crowding distance (F_{1j})
Update the achieve size
Update the position of *Mi*
Calculate the no. of flames
Evaluate the fitness function *fi*
If *(iteration==1)* then
F = sort (M)
OF = sort (OM)
Else
F = sort (Mt-1, Mt)
OF = sort (Mt-1, Mt)
End if

Table 8. Analysis of Variance for Rz.

Source	DF	Adj SS	Adj MS	*F*-Value	*P*-Value
Regression	9	225.472	25.0524	30.90	0.000
N	1	0.549	0.5493	0.68	0.422
F	1	0.008	0.0079	0.01	0.922
D	1	0.418	0.4180	0.52	0.482
N*N	1	0.737	0.7372	0.91	0.354
F*F	1	60.886	60.8865	75.10	0.000
D*D	1	0.032	0.0321	0.04	0.845
N*F	1	9.023	9.0233	11.13	0.004
N*D	1	0.173	0.1729	0.21	0.650
F*D	1	8.909	8.9093	10.99	0.004
Error	17	13.783	0.8107		
Total	26	239.254			

Table 9. Coefficients for Rz.

Term	Coef	SE Coef	*T*-Value	*P*-Value	VIF
Constant	29.6	33.8	0.88	0.393	
N	–0.0578	0.0703	–0.82	0.422	1096.00
F	–0.0048	0.0488	–0.10	0.922	190.37
D	8.4	11.7	0.72	0.482	190.38
N*N	0.000035	0.000037	0.95	0.354	1084.00
F*F	0.000885	0.000102	8.67	0.000	49.00
D*D	–1.17	5.88	–0.20	0.845	49.00
N*F	–0.000145	0.000043	–3.34	0.004	142.37
N*D	0.0048	0.0104	0.46	0.650	142.37
F*D	–0.0574	0.0173	–3.31	0.004	13.00

Table 10. Model Summary for Rz.

S	R-sq	R-sq(adj)	R-sq(pred)
0.900411	94.24%	91.19%	86.26%

For each $I = 1{:}n$ do
For each $j{=}1{:}d$ do
Update the values of r and t
Calculate the value of D w.r.t. corresponding Moth
Update $M(i,j)$ w.r.t. corresponding Moth
End For
End For
End While
Print the best solution

The pseudo-code for the Salp Swarm Optimization (SSO) algorithm is provided below.

Salp Population Initialization (P_{ij}) i=1,2,3...ns and j=1,2,3...np
While (it<=max_it)
For each salp i=1 to ns/
Calculate fitness functions *Ra, Rq and Rz*
End For
Compute non-dominated salps
Compute the best salp as the food source based on the crowding distance (F_{1j})
Update the achieve size
Calculate the value of $c1$ using $c1 = 2e^{-\left(\frac{4it}{\max_i t}\right)^2}$
Update Leader position P_{1j} using
If $c3$<0
$P_{1j} = F_{1j} - c1[(ub_j - lb_j)c2 + lb_j]$
Else
$P_{1j} = F_{1j} + c1[(ub_j - lb_j)c2 + lb_j]$
End
For each salp i=2 to ns
$P_{ij} = \frac{1}{2}(P_{ij} + P_{(i-1)j})$
End For
Check P_{ij} with in lb_j and ub_j
End While
Display the positions and its fitness values of salps from archive.

Table 11 shows the parameters used while using the GHO algorithm. Whereas Table 12 shows the parameters used in MFO and SSO algorithms respectively.

Table 11. GHO algorithm parameters.

Parameters	Value
No. of grasshopper (*ng*)	100
No. of Iterations (*nitr*)	100
Factors to control exploration and exploitation (Cmin and Cmax)	0.00004 and 1

3 Result and discussion

Figure 1 shows the Pareto chart for the standard effects taken for the surface roughness of the simple coated tool insert, i.e., Ra. The term 'A' represents the cutting speed (N), 'B' represents the feed (F) and 'C' represents the depth of cut (D). From the figure, it is found that the feed given through the tool insert had a higher affinity to increase the surface roughness. However, the combination of the feed and depth of cut provides a negligible surface roughness. Figure 2 shows the residual plots obtained for Ra. The plots reveal that the normal plot is in close correlation with the residue. Similarly, the frequency of the residue is closer to the centre. This phenomenon reveals the goodness of fit and that the optimization carried out provides reliable results. Figure 3 shows the summary of the report obtained for Ra which also provides favourable result during the study.

Figure 4a shows the RSM plot for Ra and compared it with two process parameters of turning, i.e., F and N. It is observed that for a low value of feed (F), the surface roughness Ra remains low irrespective of changes in cutting speed (N). The Ra value varies closer to unity. However, as the feed is increased, the surface roughness increases to a great extent. The surface roughness significantly increases when the cutting speed is low while maintaining a high feed. This causes the highest roughness which reaches 2.46 µm. This phenomenon is also observed for low cutting speed while maintaining a high feed. Thus, in comparison, it is found that the feed has greater influence than the cutting speed to control the surface roughness of the coated tool insert.

Figure 4b shows the RSM plot for Ra and compared it with two process parameters of turning, i.e., N and D. It is observed that for a low value of depth of cut (D), the surface roughness Ra remains low. However, the cutting speed should be maintained between 900 mm/min and 1000 mm/min to get a low surface roughness of 0.8 µm. However, further reduction in the cutting speed results in increasing the surface roughness of the coated tool insert. A considerable increase in the surface roughness of 1.35 µm is noted for a low cutting speed of 840 rpm and high depth of cut, i.e., 0.8 mm. It is inferred that the cutting speed has a greater influence on the surface roughness than the depth of the cut.

Figure 4c shows the RSM plot for Ra and compared it with two process parameters of turning, i.e., F and D. It is observed that for a low value of feed and low depth of cut, the surface roughness Ra remains considerably low i.e., 0.5 µm. While maintaining the low cutting speed, the surface roughness is observed to increase very slightly with an increase in the depth of cut. However, the surface roughness increases exponentially to 2 µm when the feed is increased irrespective of the depth of cut.

Figure 5 shows the Pareto chart for the standard effects taken for the surface roughness of the simple coated tool insert, i.e., Ra. The term 'A' represents the cutting speed (N), 'B' represents the feed (F) and 'C' represents the depth of cut (D). From the figure, it is found that the feed given through the tool insert had a very high affinity to increase the surface roughness. However, the combination of the feed and depth of cut provides a negligible surface roughness. Figure 6 shows the summary of the report obtained for Ra which also provides favourable result during the study. This phenomenon reveals the goodness of fit and that the optimization carried out provides reliable results.

Figure 7a shows the RSM plot for Rq and compared it with two process parameters of turning, i.e., F and N. It is observed that for a low value of feed (F), the surface roughness Rq remains low irrespective of changes in cutting speed (N). The Ra value varies closer to unity. However, as the feed is increased, the surface roughness increases to a great extent. The surface roughness significantly increases when the cutting speed is low while maintaining a high feed. This causes the highest roughness which reaches 3 µm. This phenomenon is also observed for low cutting speed while maintaining a high feed. Thus, in comparison, it is found that the feed has greater influence than the cutting speed to control the surface roughness of the coated tool insert.

Figure 7b shows the RSM plot for Rq and compared it with two process parameters of turning, i.e., N and D. It is observed that for a low value of depth of cut (D), the surface roughness Rq remains low i.e., 0.5 µm. However, the cutting speed should be maintained at 1050 mm/min to get a low surface roughness of 0.8 µm. However, further reduction in the cutting speed results in increasing the surface roughness of the coated tool insert. A considerable increase in the surface roughness of 1.75 µm is noted for a low cutting speed of 840 rpm and high depth of cut, i.e., 0.8 mm. It is inferred that the cutting speed has a greater influence on the surface roughness than the depth of cut.

Figure 7c shows the RSM plot for Rq and compared it with two process parameters of turning, i.e., F and D. It is observed that for a low value of feed and low depth of cut, the surface roughness Rq remains considerably low i.e., 0.5 µm. While maintaining the low cutting speed, the surface roughness is observed to increase very slightly with an increase in the depth of cut. However, the surface roughness increases exponentially to 2.5 µm when the feed is increased irrespective of the depth of cut.

Figure 8 shows the Pareto chart for the standard effects taken for the surface roughness of the simple coated tool insert, i.e., Rz. The term 'A' represents the cutting speed (N), 'B' represents the feed (F) and 'C' represents the depth of cut (D). From the figure, it is found that the feed given through the tool insert had a very high affinity to increase the surface roughness. However, the combination of the feed and depth of cut provides a negligible surface roughness. Figure 9 shows the residual plots obtained for Rz. The plots reveal that the normal plot is in close

Table 12. MFO and SSO algorithm parameters.

MFO algorithm		SSO algorithm	
Parameter	Value	Parameter	Value
Location of moth closest to flame (t)	-1 to −2	C1-coefficient to control exploration and exploitation	$2e^{-\left(\frac{4*it}{nitr}\right)^2}$
Updated mechanism	Logarithmic Spiraled	C2 and C3	Random value between 0 and 1
Moths (N)	30	No. of Salps (N)	30
No. of iterations ($nitr$)	100	No. of iterations ($nitr$)	100

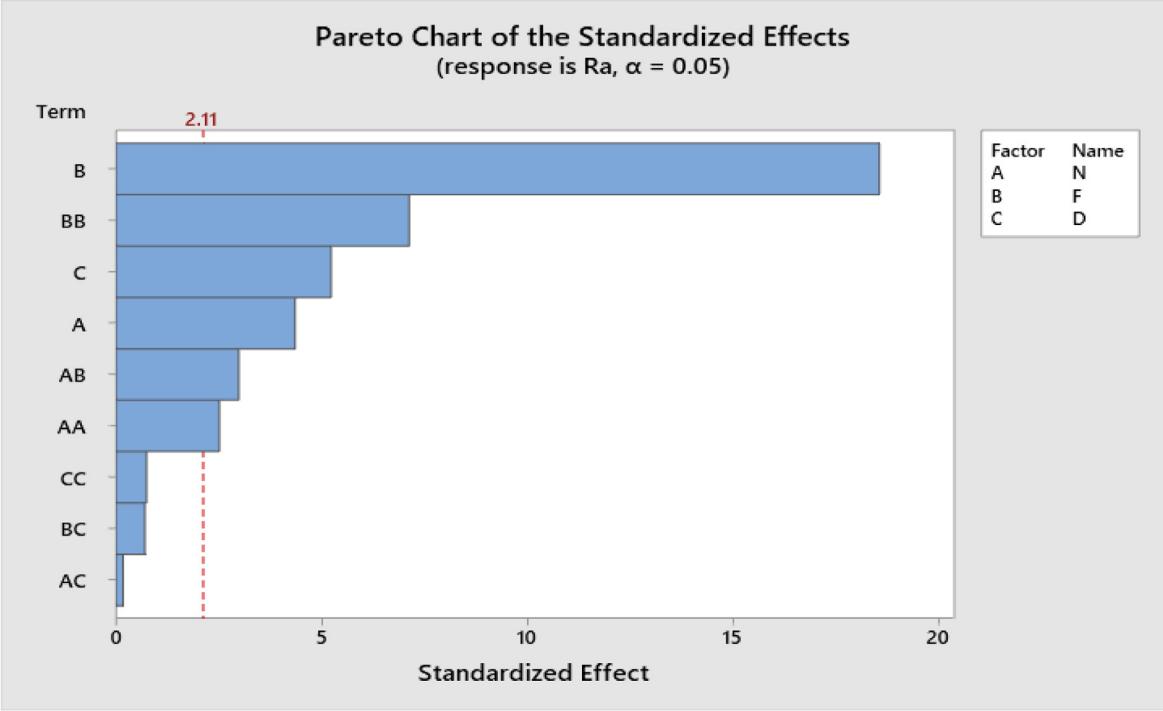

Fig. 1. Pareto chart for the standard effects for Ra.

correlation with the residue. Similarly, the frequency of the residue is closer to the centre. Figure 10 shows the summary of the report obtained for Ra which also provides favourable result during the study. This phenomenon reveals the goodness of fit and that the optimization carried out provides reliable results.

Figure 11a shows the RSM plot for Rz and compared it with two process parameters of turning, i.e., F and N. It is observed that for a moderate feed of 100 mm/min, the surface roughness Rz remains low irrespective of changes in cutting speed (N). Reduction in the feed increases the surface roughness to 5 μm. On the other hand, increasing the feed to 175 mm/min results in a tremendous increase in the surface roughness, i.e., 12.5 μm. Thus, in comparison, it is found that the feed has greater influence than the cutting speed to control the surface roughness of the coated tool insert.

Figure 11b shows the RSM plot for Rz and compared it with two process parameters of turning, i.e., N and D. It is observed that for a low value of depth of cut (D), the surface roughness Rz remains low i.e., 3.25 μm. However, the cutting speed should be maintained at 1050 mm/min to get a low surface roughness of 0.8 μm. Further reduction in the cutting speed results in increasing the surface roughness of the coated tool insert. A considerable increase in the surface roughness of 5.85 μm is noted for a low cutting speed of 840 rpm and high depth of cut, i.e., 0.8 mm. It is inferred that the cutting speed has a greater influence on the surface roughness than the depth of cut.

Figure 11c shows the RSM plot for Rz and compared it with two process parameters of turning, i.e., F and D. It is observed that for a low value of feed and low depth of cut, the surface roughness Rz remains considerably low i.e., 2 μm. While maintaining the low cutting speed, the surface

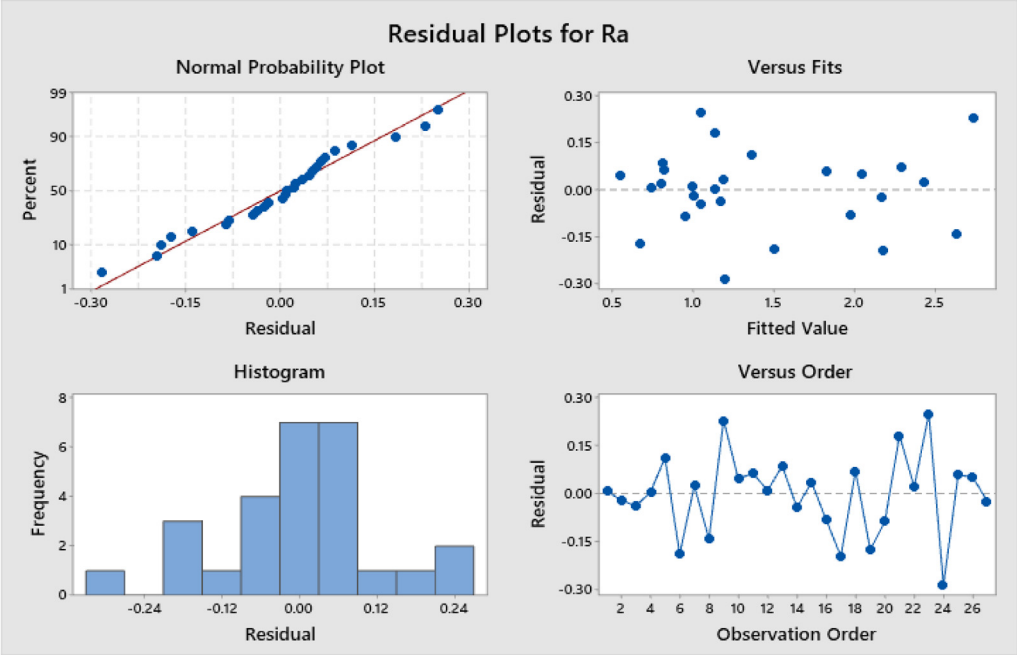

Fig. 2. Residual plots for Ra.

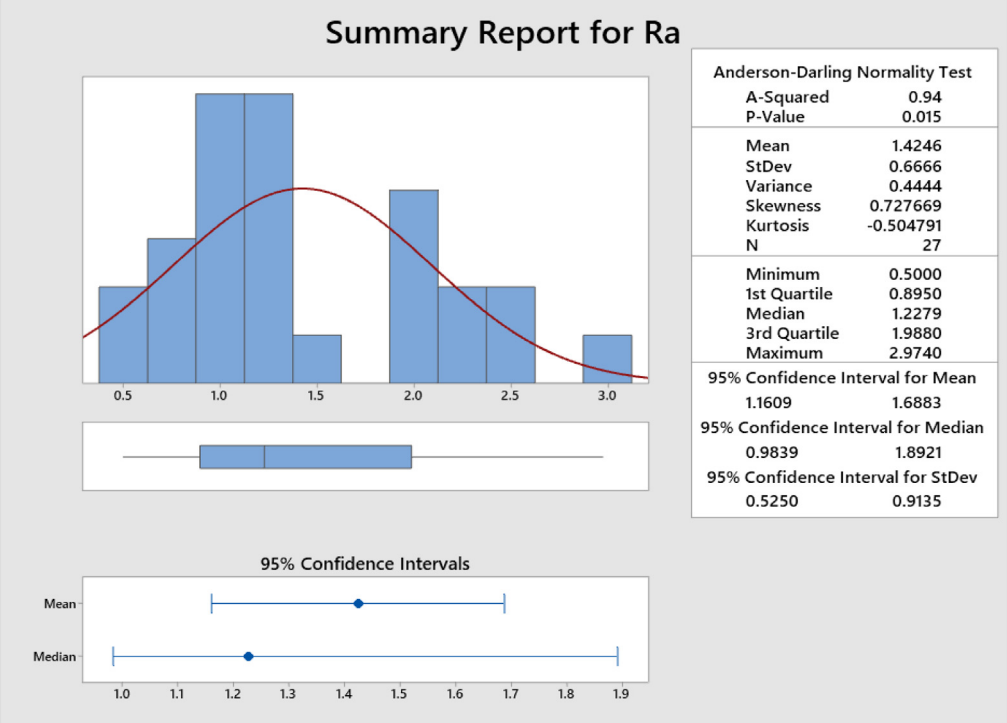

Fig. 3. Summary report for Ra.

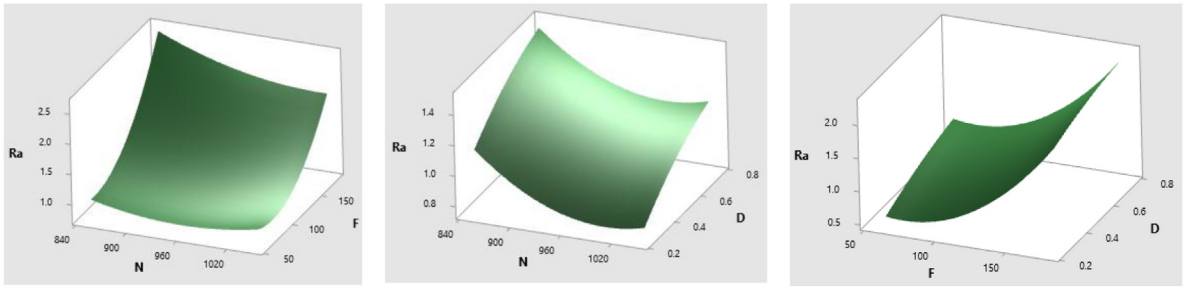

Fig. 4. RSM for Ra.

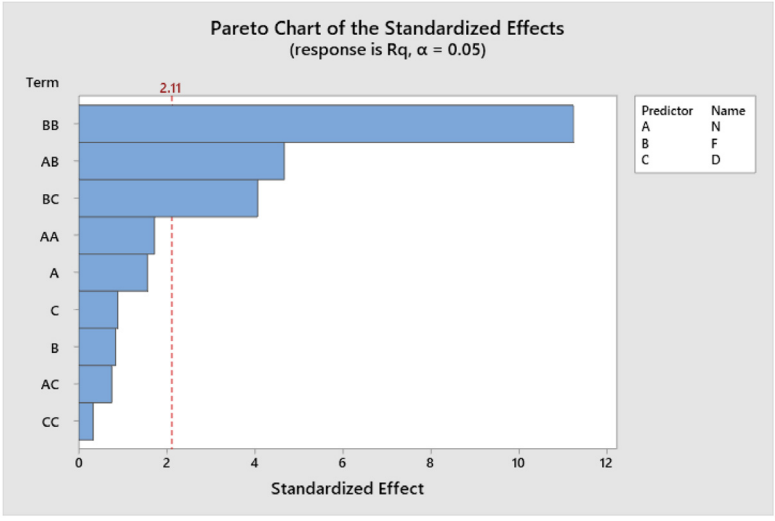

Fig. 5. Pareto chart for the standard effects for Rq.

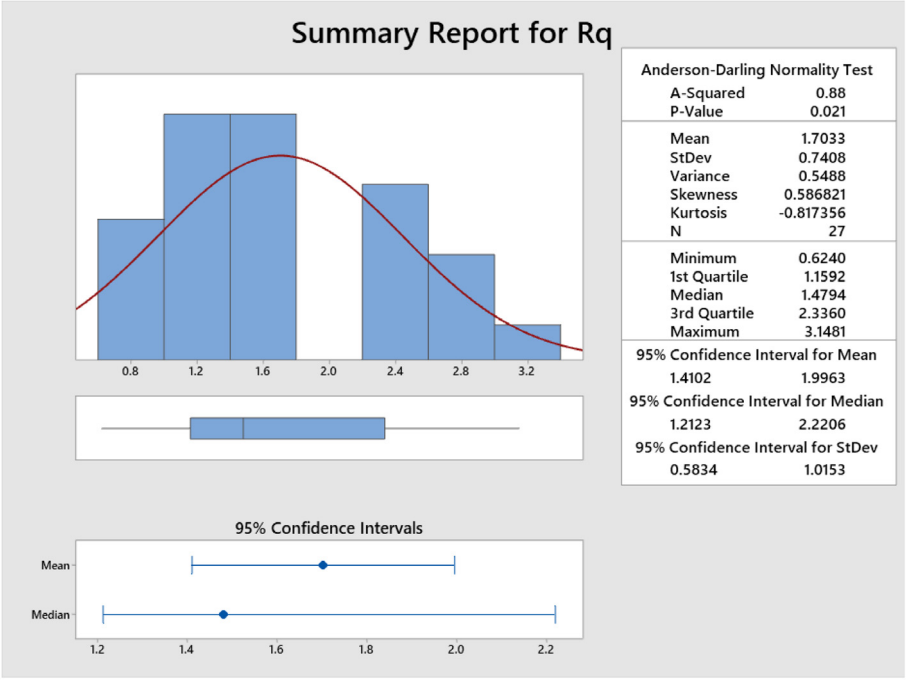

Fig. 6. Summary report for Rq.

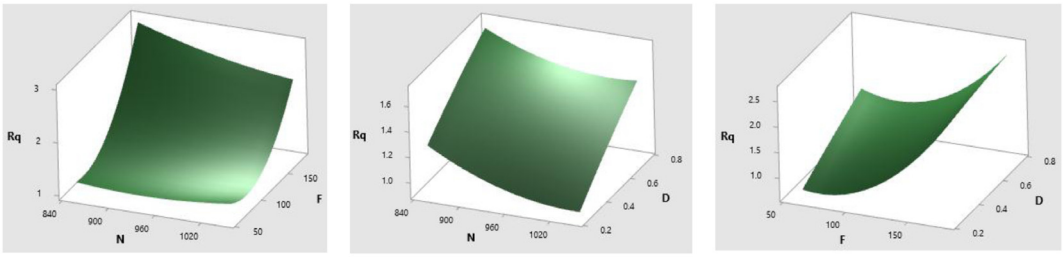

a. Rq vs F,N b. Rq vs D, N c. Rq vs D, F

Fig. 7. RSM for Rq.

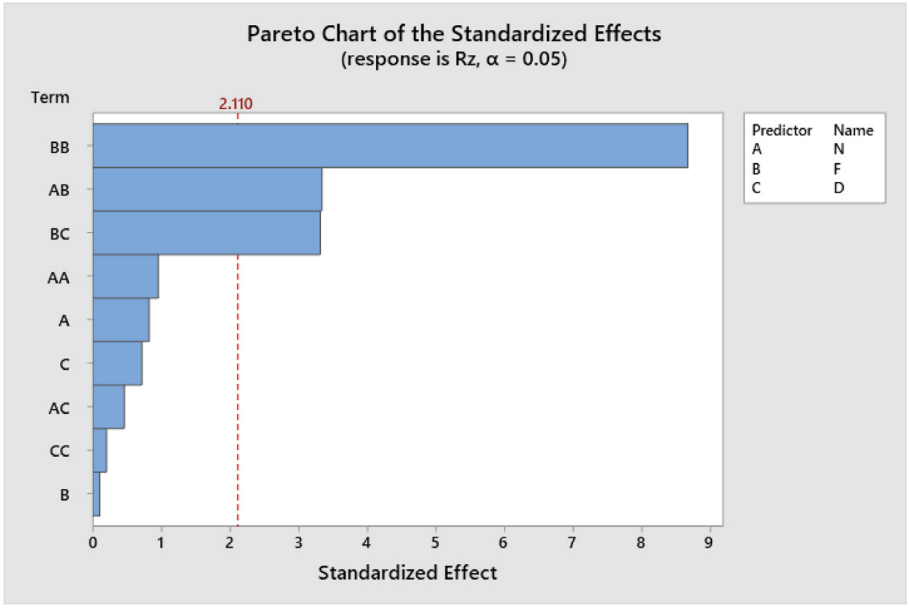

Fig. 8. Pareto chart for the standard effects for Rz.

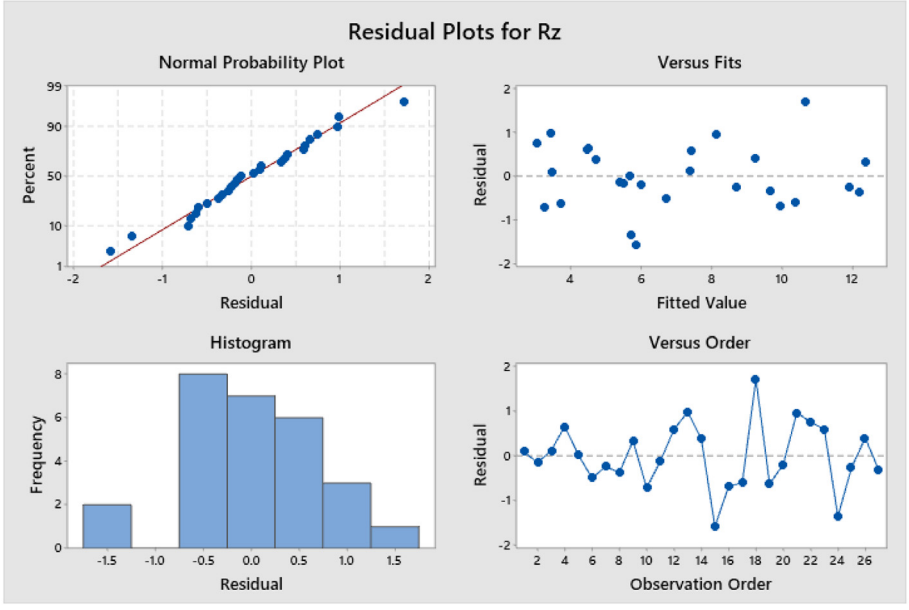

Fig. 9. Residual plots for Rz.

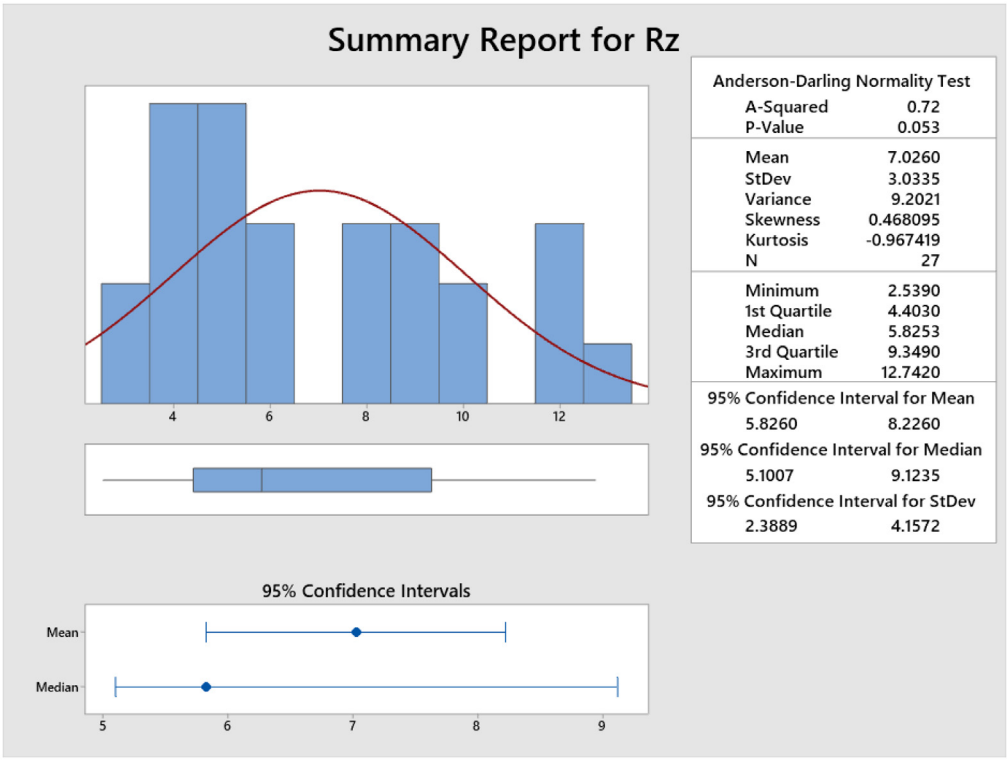

Fig. 10. Summary report for Rz.

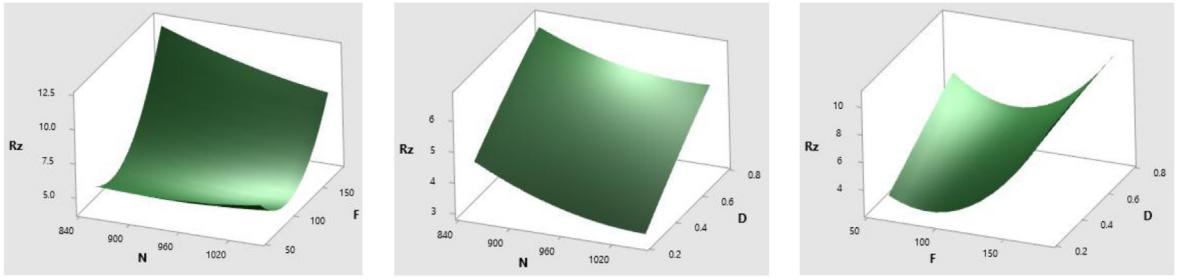

a. Rz vs F,N b. Rz vs D, N c. Rz vs D, F

Fig. 11. RSM for Rz.

roughness is observed to increase very slightly with an increase in the depth of cut. However, the surface roughness increases exponentially to 10 μm when the feed is increased irrespective of the depth of cut.

The three different optimization techniques, i.e., GHO, MFO, and SOO were used to find the influence of the process parameters i.e., cutting speed, feed and depth of cut on the surface roughness of the coated tool insert. The surface roughness (Ra) of the simple coated tool insert is compared with the post-coated inserts that were dipped in liquid nitrogen for 24h (Rq) and 36h (Rz) respectively. Table 13 shows the optimum process parameters of the three different surface roughness measured using the GHO technique. It is inferred that the post-treatment increased the brittleness of the tool insert. Because of this the strength of the tool insert increased but underwent microscopic abrasion during the turning process. As the result, the surface roughness increased proportionally with the time taken by the tool insert inside the liquid nitrogen. Tables 14 and 15 show the optimum process parameters of the three different surface roughness measured using MFO and SSO techniques respectively. Each of these techniques projected a different value of surface roughness for the given combination of the process parameters. Comparatively, the MFO technique delivered are having less deviation from the initial value of the surface roughness.

Figures 12 to14 show the summary of the three different optimization techniques used in this study. The spatial distribution obtained during the optimization is projected through the respective plots. The GHO plots show that it is skewed towards the right which shows that the values do

Table 13. Optimum process parameters using GHO.

N	F	D	Ra	Rq	Rz
1004	93	0.25	0.60648	0.94139	2.41554
969	83	0.25	0.56393	0.89275	2.48878
972	84	0.25	0.56582	0.89574	2.47529
970	81	0.25	0.55853	0.88820	2.51967
972	83	0.25	0.56386	0.89393	2.48339
973	83	0.25	0.56377	0.89409	2.48290
988	87	0.25	0.57433	0.90813	2.44307
967	78	0.25	0.55334	0.88297	2.58738
974	79	0.25	0.55443	0.88610	2.56090
980	83	0.25	0.56382	0.89615	2.47951
972	82	0.25	0.55990	0.89021	2.50630
978	84	0.25	0.56419	0.89620	2.47735
992	89	0.25	0.58270	0.91703	2.42713
953	77	0.25	0.55886	0.88071	2.59645
975	80	0.25	0.55710	0.88879	2.52832
970	84	0.25	0.56676	0.89621	2.47374
989	90	0.25	0.58530	0.91965	2.42304
974	85	0.25	0.56914	0.89977	2.46092
981	86	0.25	0.57119	0.90382	2.44968
968	84	0.25	0.56659	0.89526	2.47817
982	86	0.25	0.57188	0.90476	2.44755

Table 14. Optimum process parameters using MFO.

N	F	D	Ra	Rq	Rz
988	93	0.251157	0.60104	0.93688	2.42995
1002	93	0.250168	0.60552	0.94068	2.41658
1001	93	0.2501	0.60457	0.93984	2.41604
1001	92	0.250201	0.59815	0.93290	2.41802
998	91	0.250235	0.59500	0.92994	2.41858
996	92	0.250674	0.59830	0.93375	2.42090
1008	93	0.25	0.60621	0.94026	2.41705
992	92	0.250051	0.59664	0.93199	2.41807
995	91	0.250098	0.59141	0.92625	2.41904
984	91	0.250002	0.59124	0.92564	2.42300
996	93	0.250239	0.60197	0.93769	2.41822
1004	92	0.250692	0.60187	0.93650	2.42173
995	94	0.250044	0.60323	0.93912	2.41800
999	93	0.250126	0.60284	0.93825	2.41629
1001	92	0.250102	0.59779	0.93251	2.41738
993	92	0.250118	0.59461	0.92978	2.41812
989	92	0.250117	0.59349	0.92850	2.42000
997	93	0.25014	0.60364	0.93941	2.41750
999	92	0.250049	0.59823	0.93325	2.41607
992	92	0.250658	0.59815	0.93373	2.42236
998	93	0.250079	0.60087	0.93625	2.41602

Table 15. Optimum process parameters using SSO.

N	F	D	Ra	Rq	Rz
985	89	0.25	0.58099	0.91473	2.42868
1009	89	0.25	0.59566	0.92874	2.43128
997	91	0.25	0.59356	0.92839	2.41740
1003	93	0.25	0.60258	0.93741	2.41547
996	92	0.25	0.59464	0.92969	2.41661
989	90	0.25	0.58574	0.92011	2.42267
987	88	0.25	0.57865	0.91247	2.43223
1012	91	0.25	0.60378	0.93651	2.42474
995	93	0.25	0.59864	0.93408	2.41636
976	80	0.25	0.55730	0.88924	2.52654
995	91	0.25	0.59014	0.92489	2.41911
983	90	0.25	0.58477	0.91836	2.42665
989	85	0.25	0.56982	0.90374	2.46173
978	85	0.25	0.56747	0.89942	2.46281
985	87	0.25	0.57508	0.90842	2.43934
985	86	0.25	0.57258	0.90592	2.44604
973	86	0.25	0.56999	0.90046	2.45914
1006	91	0.25	0.60074	0.93468	2.41895
1006	94	0.25	0.61178	0.94662	2.41671
990	88	0.250293	0.58060	0.91479	2.43222
989	84	0.25	0.56747	0.90142	2.47266

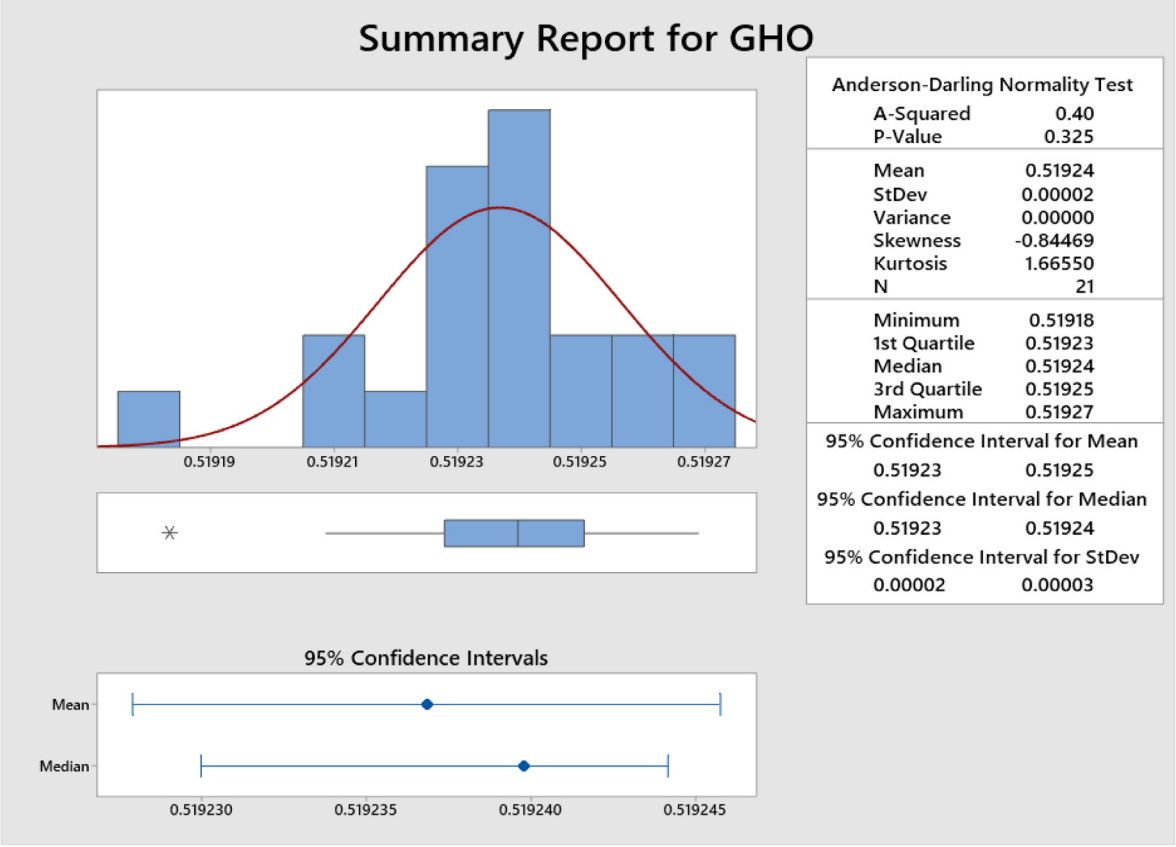

Fig. 12. Distribution plot for GHO technique.

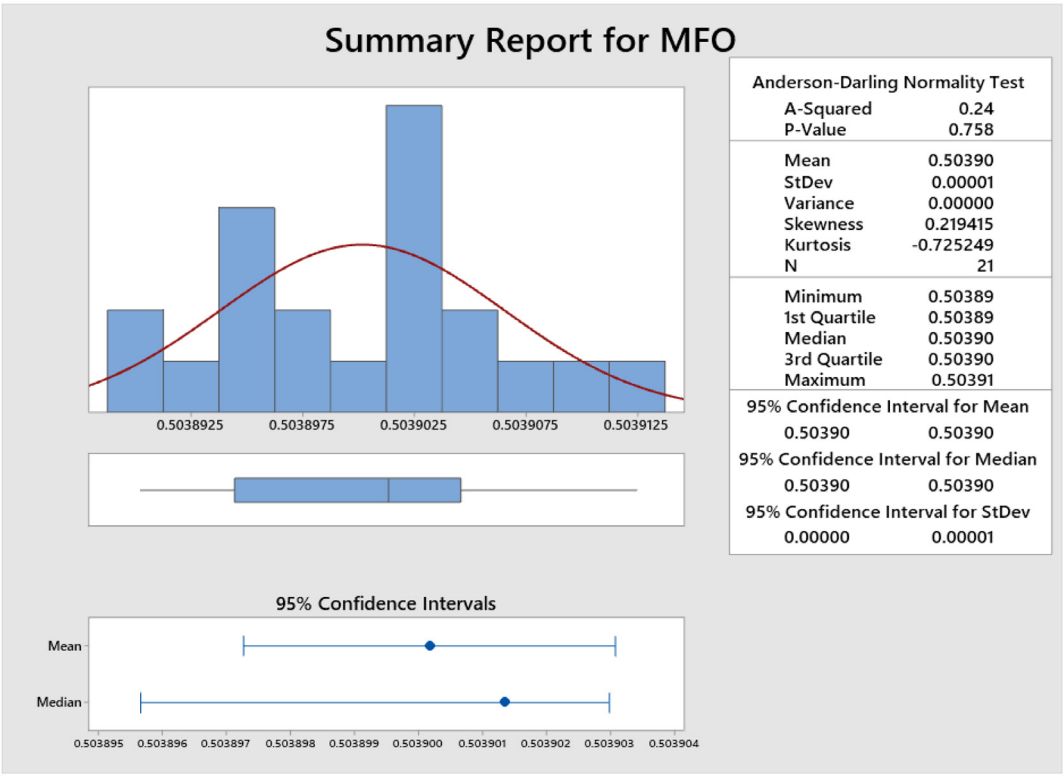

Fig. 13. Distribution plot for MFO technique.

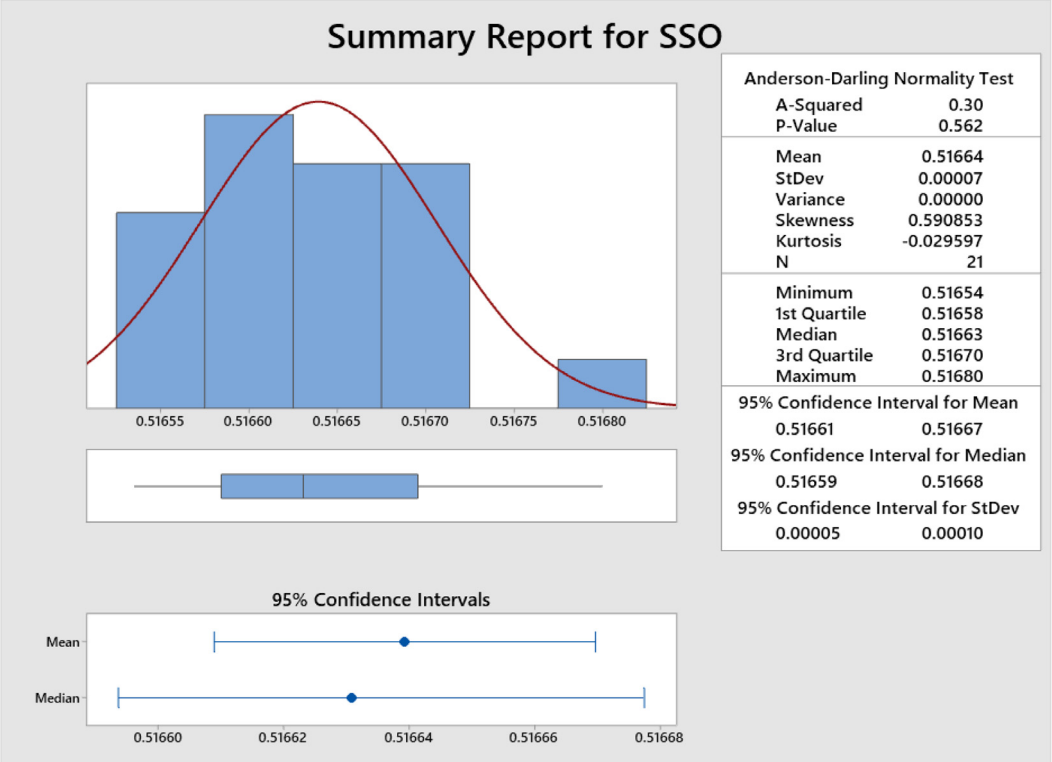

Fig. 14. Distribution plot for SSO technique.

Table 16. Parameter and surface roughness for algorithm.

Algorithm	N	F	D	Ra	Rq	Rz
GHO	967.3878	77.50464	0.25	0.553337	0.882965	2.587379
MFO	984.4647	91.40078	0.250002	0.591239	0.925636	2.422999
SSO	976.1378	80.4994	0.25	0.557304	0.889238	2.526539

Table 17. Statistical performance of algorithms.

Algorithm	IGD	SP
GHO	0.011969	0.010034
MFO	0.003057	0.002026
SSO	0.011294	0.012248

Table 18. Surface roughness using different algorithm.

RNO.	GHO	MFO	SSO
1	0.519183	0.503901	0.516645
2	0.51924	0.503891	0.516598
3	0.519236	0.503892	0.516595
4	0.519252	0.503901	0.516564
5	0.51924	0.503906	0.516591
6	0.519241	0.503902	0.516625
7	0.519225	0.50389	0.516656
8	0.519269	0.503903	0.516566
9	0.519266	0.503911	0.516578
10	0.519242	0.503912	0.5168
11	0.519249	0.503896	0.516608
12	0.519241	0.503898	0.516631
13	0.519212	0.503894	0.516708
14	0.519256	0.503894	0.516717
15	0.519257	0.503902	0.516673
16	0.519235	0.503906	0.516687
17	0.519209	0.503908	0.516705
18	0.519231	0.503894	0.516572
19	0.519228	0.503901	0.516535
20	0.519235	0.503903	0.516649
21	0.519227	0.503897	0.516725

not converge. On the other hand, the SSO plot shows that it is skewed towards the left which shows that the values do not converge. However, the MFO technique shows that its values are converging well.

Table 16 shows the process parameters that delivered lower surface roughness for the simple coated tool insert and the two post-processed tool inserts. These values were compared against the three algorithms used in this study. It is revealed that the simple coated tool insert exhibited lower surface roughness irrespective of the algorithm used. Table 17 shows the statistical performance of the three different algorithms considered for this study. From the table, it is found that the MFO technique delivered lower IGD and SP values than the other techniques. Hence, the values assigned to the process parameters of the MFO technique were incorporated into the GHO and SSO techniques. Table 18 shows the variation in surface roughness of the simple coated tool inserts under various process parameters. It is found that the surface roughness minimised considerably in the GHO and SSO techniques after incorporating the values of the MFO technique respectively.

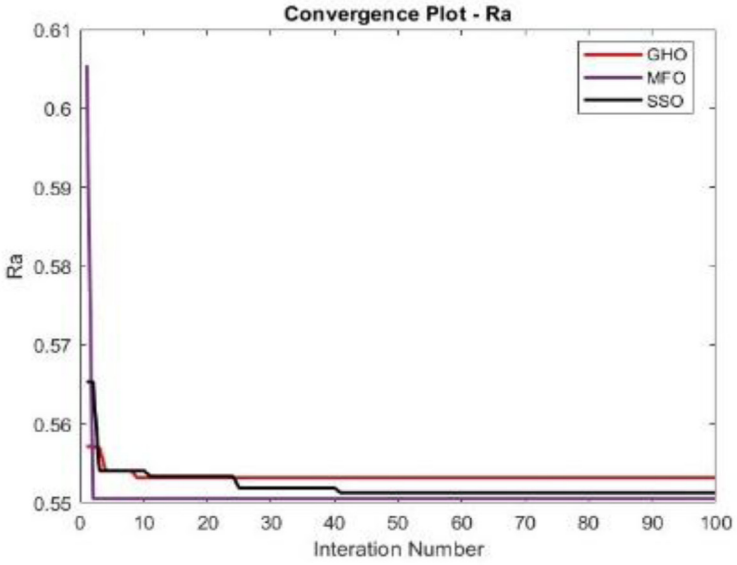

a. Ra

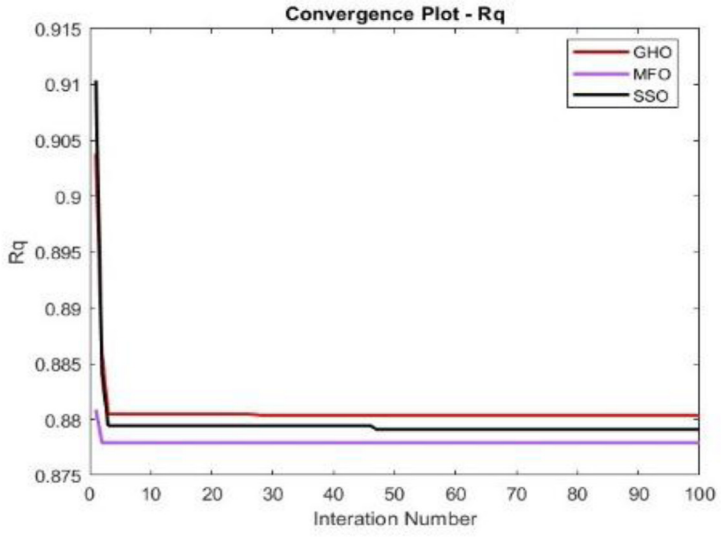

b. Rq

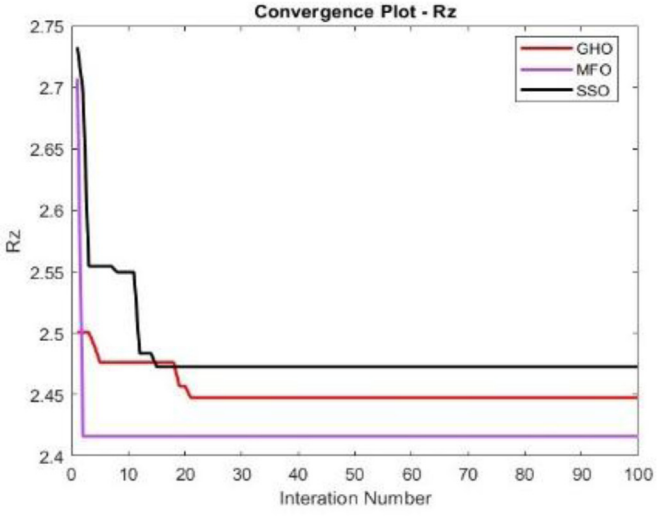

c. Rz

Fig. 15. Convergence plots.

Figure 15 shows the convergence plots of Ra, Rq, and Rz for the three different algorithms respectively. It is found that the MFO technique converged quickly irrespective of the process and post-process used on the coated tool insert.

4 Conclusion

The surface roughness of the tungsten carbide-coated tool inserts subjected to turning operation was compared to treated inserts that were immersed in liquid nitrogen for 24 h and 36 h respectively. The ANOVA optimization technique delivered compatible results of the surface roughness with the Taguchi L27 technique. Response Surface Methodology revealed that the tool feed had a higher influence on the surface roughness than the cutting tool speed and depth of cut. It was revealed that for high cutting speed when the tool feed and depth of cut were low the surface roughness was around 0.5 μm. Tool inserts subjected to strengthening using liquid nitrogen became brittle and as the result, they exhibited high surface roughness of around 12.5 μm. Out of the three techniques, the Moth Flame Optimization showed good convergence. The Moth Flame Optimization technique exhibited values that were having good correlation with the ANOVA. It is concluded that for the turning process parameters of 984.46 rpm, 91.4 mm/min and 0.25 mm depth of cut, the surface roughness of the simple coated tool insert was 0.59 μm.

Author's contributions

Karthick Muniyappan: Literature survey, Preliminary investigation, Methodology of the research, Data interpretation, Inference of the study, Result and discussion
Lenin Nagarajan: Supervision of the study, Selection of optimization techniques, ANOVA study, Manuscript correction, Conclusion

References

1. A. Yadav, A. Bangar, R. Sharma, D. Pal, Optimization of turning process parameters for their effect on En 8 material work piece hardness by using Taguchi parametric optimization method, Int. J. Mech. Ind. Eng. (IJMIE) **1**, 17–33 (2015), ISSN No 2231–6477
2. S. Shivade, S. Bhagat, S. Jagdale, A. Nikam, P. Londhe, Optimization of machining parameters for turning using Taguchi approach, Int. J. Recent Technol. Eng. (IJRTE) 3:**1**, 145–149 (2014) ISSN: 2277–3878
3. R.R. Deshpande, R. Pant, Optimization of process parameters for CNC turning using Taguchi methods for en-8 alloy steel with coated/uncoated tool inserts, Int. Res. J. Eng. Technol. **04**, 180–188 (2017)
4. S.V. Alagarsamy, P. Raveendran, S. Arockia Vincent Sagayaraj, S. Tamil Vendan, Optimization of machining parameters for turning of aluminium alloys 7075 using Taguchi method, Int. Res. J. Eng. Technol. **6**, 22–38 (2016)
5. S. Lakshmanan, M. Pradeep Kumar, M. Dhananchezian, N. Yuvaraj, Investigation of monolayer coated WC inserts on turning Ti-alloy, **35**:7, 826–835, DOI: 10.1080/10426914.2020.1711930
6. E.-O. Ezugwu, Z.-M. Wang, Titanium alloys and their machinability-a review, J. Mater. Process. Technol. **68**, 262–274 (1997)
7. Y. Xiaoping, L.-C. Richard, Machining titanium and its alloys, Int. J. Mach. Sci. Technol. **3**, (1999)
8. C. Kainz, N. Schalk, M. Tkadletz, C. Mitterer, C. Christoph, Microstructure and mechanical properties of CVD TiN/TiBN multilayer coatings, Surf. Coat. Technol. **370**, 311–319 (2019)
9. S. Alborz, D. Vimal, S.-T. Newman, Investigation of the effects of cryogenic machining on surface integrity in CNC end milling of Ti-6Al-4V titanium alloy, J. Manuf. Processes. **21**, 172–179 (2016)
10. K. Emel, Nose radius and cutting speed effects during milling of AISI 304 material, Mater. Manuf. Processes. **32**, 185–192 (2017)
11. A. Fernández-Valdivielso, L.N. López De Lacalle, G. Urbikain, A. Rodriguez, Detecting the key geometrical features and grades of carbide inserts for the turning of nickel-based alloys concerning surface integrity, Proc. Inst. Mech. Eng., Part C: J. Mech. Eng. Sci. **230**, 3725–3742 (2016)
12. A. Gandarias, L.N.L. de Lacalle, X. Aizpitarte, A. Lamikiz, Study of the performance of the turning and drilling of austenitic stainless steels using two coolant techniques, Int. J. Mach. Mach. Mater. **3**, 1–17 (2008)
13. O. Pereira, A. Rodríguez, A. Fernández-Valdivielso, J. Barreiro, A.I. Fernández-Abia, L.N. López-De-Lacalle, Cryogenic hard turning of ASP23 steel using carbon dioxide, Proc. Eng. **132**, 486–491 (2015)
14. R. Polvorosa, A. Suárez, L.N.L. de Lacalle, I. Cerrillo, A. Wretland, F. Veiga, Tool wear on nickel alloys with different coolant pressures: comparison of alloy 718 and Waspaloy, J. Manuf. Process. **26**, 44–56 (2017)
15. F.J. Amigo, G. Urbikain, L.N. López de Lacalle, O. Pereira, P. Fernández-Lucio, A. Fernández-Valdivielso, Prediction of cutting forces including tool wear in high-feed turning of Nimonic® C-263 superalloy: a geometric distortion-based model, Measurement **211**, 112580 (2017)
16. X. Zhang, T. Yu, P. Xu, J. Zhao, In-process stochastic tool wear identification and its application to the improved cutting force modeling of micro milling, Mech. Syst. Signal Process. **164**, 108233 (2022)
17. V. Sivalingam, J. Sun, S.K. Mahalingam, L. Nagarajan, Y. Natarajan, S. Salunkhe, E.A. Nasr, J. Paulo Davim, H.M.A. M. Hussein, Optimization of process parameters for turning Hastelloy X under different machining environments using evolutionary algorithms: a comparative study, Appl. Sci. **11**, 9725 (2021)
18. J.D.J. Dhilip, J. Jeevan, D. Arulkirubakaran, M. Ramesh, Investigation and optimization of parameters for hard turning of OHNS steel, Mater. Manuf. Processes. **35**, 1113–1119 (2020)
19. R. Rana, L. Krishnaia, Q. Murtaza, R.S. Walia, Optimizing the machining performance of CNC tools inserts coated with diamond like carbon coatings under the dry cutting environment, J. Eng. Res. - ICARI Special Issue, **4**, 142–152 (2021). https://doi.org/10.36909/jer.ICARI.15327

20. A. Das, S.R. Das, J.P. Panda, A. Dey, K.K. Gajrani, N. Somani, N. Gupta, Machine learning based modelling and optimization in hard turning of AISI D6 steel with newly developed AlTiSiN coated carbide tool, Comp. Sci. **15**, 43–54 (2022). https://doi.org/10.48550/arXiv.2202.00596
21. A.S. Sobh, E.M. Sayed, A.F. Barakat, R.N. Elshaerr, Turning parameters optimization for TC21 Ti-alloy using Taguchi technique, J. Basic Appl. Sci. **12**, 1–25 (2023)
22. D. Vukelic, M. Prica, V. Ivanov, G. Jovicic, I. Budak, O. Luzanin, Optimization of surface roughness based on turning parameters and insert geometry, Int. J. Simul. Model **21**, 417–428 (2022)
23. P. Kamble, S. Kulkarni, S. Marathe, U. Kamble, S.B. Barve, H. Mech Dept, Review of tool life optimization methods and their effectiveness for turning inserts, Int. J. Res. Eng. Appl. Manag. **5**, 85–88 (2019). https://doi.org/10.35291/2454-9150.2020.0114
24. E. Nas, N.A. Özbek, Optimization of the machining parameters in turning of hardened hot work tool steel using cryogenically treated tools, Surf. Rev. Lett. 27:**5**, 26–42 (2020). https://doi.org/10.1142/S0218625×19501774
25. S.H. Tomadi, N.F.H.A. Halim, A.N. Dahnel, A.S. Rosman, G. Umma Sankar, L.J. Eng, Optimization study on width of cut and cutting-edge radius during side milling of DAC 55 steel, Lect. Notes Mech. Eng. **33**, 214–216 (2022)
26. M. Akgün, F. Kara, Analysis and optimization of cutting tool coating effects on surface roughness and cutting forces on turning of AA 6061 alloy, Adv. Mater. Sci Eng. **2021**, 1–12 (2021)
27. Turning studies of AISI 1018 steel using multi objective optimization. *International Conference on Computational Intelligence for Smart Power System and Sustainable Energy*, CISPSSE **5**, 29–32 (2020). https://doi.org/10.1109/CISPSSE49931.2020.9212247

Cite this article as: Karthick Muniyappan, Lenin Nagarajan, Parameter optimization of titanium-coated stainless steel inserts for turning operation, Int. J. Simul. Multidisci. Des. Optim. **14**, 19 (2023)